Cooper et al. (2012): Large normal-sense displacement on the South Tibetan fault system in the eastern Himalaya

GSA Data Repository Item DR1

ASTER files downloaded from the USGS Land Processes Distributed Active Archive Center (https://lpdaac.usgs.gov/)

File name – L1B data[a]	File name – AST05 data[b]	Date of acquisition	Scene center (Lat, Long)
AST_L1B_00301062005045226_20101101191054_1606	AST_05_00301062005045226_20101101191634_5846	2005-01-06	28°09'21"N, 89°39'44"E
AST_L1B_00311012000050026_20101101191054_1608	AST_05_00311012000050026_20101101191744_6808	2000-11-01	27°23'57"N, 88°49'16"E
AST_L1B_00311012000050035_20101101191134_2209	AST_05_00311012000050035_20101101191654_5894	2007-12-14	27°37'19"N, 89°32'15"E
AST_L1B_00312082005045225_20101101191114_1878	AST_05_00312082005045225_20101101191744_6810	2005-12-08	27°38'41"N, 89°23'25"E
AST_L1B_00312082005045234_20101101191114_1876	AST_05_00312082005045234_20101101191614_5708	2005-12-08	27°06'47"N, 89°15'04"E
AST_L1B_00312092002044846_20101101191134_2206	AST_05_00312092002044846_20101101191604_5672	2002-12-09	27°18'59"N, 89°24'57"E
AST_L1B_00312142007045318_20101101191104_1751	AST_05_00312142007045318_20101101191454_5377	2000-11-01	27°55'58"N, 88°56'57"E

[a]Registered radiance at sensor: Surface radiance data with radiometric and geometric coefficients applied.
[b]Surface emissivity: NASA temperature-emissivity separation algorithm applied to atmospherically corrected surface radiance data.

Cooper et al. (2012): Large normal-sense displacement on the South Tibetan fault system in the eastern Himalaya

GSA Data Repository Item DR2

ASTER scene processing steps

1. Select scenes

Only images taken prior to the 2008 failure of the shortwave infrared channels were selected since the spectral mask used to identify ice (NDSII – see step 3) is dependent on Band 4 (1.6–1.7μm), which is the first band of the shortwave infrared detector. In addition, scenes were selected on the basis of minimal cloud cover (≤ 11%) in order to reveal as much of the ground geology as possible.

2. Remove systematic noise

Column- and row- correlated band-independent noise, known as "plaid" is common in ASTER radiance and thermal infrared emissivity data, and was removed prior to further processing.

Statistical methods for systematically removing row-correlated noise (on the order of 5–10 pixels wide) were employed to highlight the spectral variability in the scenes that may be obscured by instrumental noise. Enhanced row-correlated noise (occurring perpendicular to the along track direction) may be due to some small variability in the detector readout or residual voltage. This image artifact is identifiable by row correlated color variability in decorrelation stretch images (Gillespie, 1986), as this effect is band independent.

Band-correlated noise would have the effect of raising the overall brightness of the line and not the brightness of a single band. To correct for this instrumental effect, a row average is taken of every 256-line segment of the image for each band, ignoring data values varying more than 15% from the local mean to systematically exclude regions with excessively high or low values that would dominate the row average data. This data is then low pass filtered with a boxcar kernel of 301 pixels. Finally, the smoothed row average is subtracted from the original row average and the result is very nearly the row-correlated noise, which can then be removed from the data.

3. Apply data exclusion masks to remove unwanted pixels from the TIR data

Each scene was re-sampled to the same resolution as the 90 m ASTER thermal infrared channels using a bilinear interpolation algorithm. Then, three distinct data exclusion masks were created as follows: (VNIR = visible/near infrared; SWIR = short wave infrared)

(a) Normalized Difference Vegetation Index (NDVI) mask

Vegetation was identified using the Normalized Difference Vegetation Index (NDVI) [NASA Earth Observatory, earthobservatory.nasa.gov], where index values > ~0.20 (highly vegetated areas) were excluded.

$$NDVI = \frac{VNIR\ Band\ 3 - VNIR\ Band\ 2}{VNIR\ Band\ 3 + Band\ 2}$$

(b) Normalized Difference Snow and Ice Index (NDSII) mask

Snow and ice were identified using the Normalized Difference Snow and Ice Index (NSDII) (Xiao et al., 2001) where index values < ~0.48 and > ~0.80 were excluded. This mask was also effective at masking bodies of water such as lakes.

$$NDSII = \frac{VNIR\ Band\ 1 - SWIR\ Band\ 1}{VNIR\ Band\ 1 + SWIR\ Band\ 1}$$

(c) Cloud mask

Clouds were identified using absolute reflectance in visible/near infrared Band 1 (0.52-0.60μm) where values > 40–80 $Wm^{-2}sr^{-1}um^{-1}$ were excluded.

$$CLOUD = VNIR\ Band\ 1$$

Pixels in the thermal infrared data that had any value in the three data exclusion masks outside the established range were excluded from the stretched data. This was done in an effort to enhance the variability of the decorrelation stretch in locations that were not cloudy, covered by vegetation, snow and ice, or water. By excluding four significant components in the scene, it is assumed that the remainder of the variability in the image is primarily due to the mineralogy of the rocks on the ground.

4. Apply a decorrelation stretch to the masked scene

The decorrelation stretch was applied to enhance (stretch) the color differences found in the three TIR bands (see Gillespie, 1986). Several different band combinations were created (see DR4 and DR5) to highlight the different mineralogies identifiable with this technique.

References cited

Gillespie, A.R., Kahle, A.B., and Walker, R.E., 1986, Color Enhancement of Highly Correlated Images. I. Decorrelation and HSI Contrast Stretches: Remote Sensing of Environment, v. 20, p. 209–235.

NASA Earth Observatory site, accessed March 2011, Measuring Vegetation (NDVI & EVI), http://earthobservatory.nasa.gov/Features/MeasuringVegetation/measuring_vegetation_2.php

Xiao, X., Shen, Z., and Qin, X., 2001, Assessing the potential of VEGETATION sensor data for mapping snow and ice cover: a Normalized Difference Snow and Ice Index: International Journal of Remote Sensing, v. 22, no. 13, p. 2479–2487.

Cooper et al. (2012): Large normal-sense displacement on the South Tibetan fault system in the eastern Himalaya

GSA Data Repository Item DR3

Location of ASTER scenes used for this study. The scenes are constructed from the visible/near infrared bands 3N, 2, and 1 mapped as red, green, and blue, respectively. The scenes are superimposed on a digital elevation model of the region.

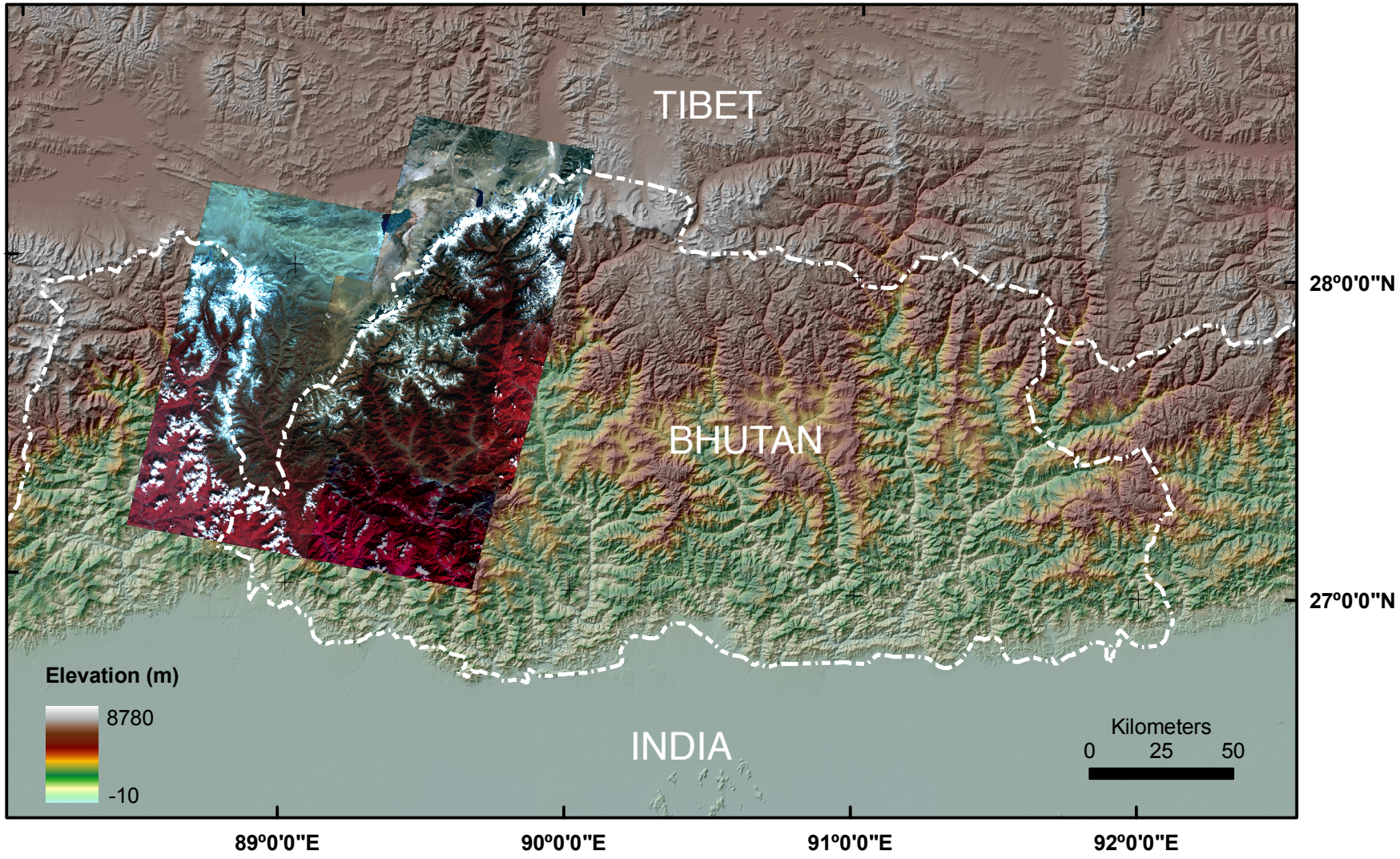

Cooper et al. (2012): Large normal-sense displacement on the South Tibetan fault system in the eastern Himalaya

GSA Data Repository Item DR4

Decorrelation stretched emissivity mosaic of the seven masked (water, ice, and vegetation removed) ASTER AST05 scenes constructed from the thermal infrared bands 14 (10.95–11.65µm), 13 (10.25–10.95µm), and 11 (8.475–8.825µm) mapped as red, green, and blue, respectively. In this stretch, the bands were chosen to highlight the spectral variability in the mountainous regions of the image where pelitic and gneissic rocks are purple, and calcareous marbles and quartz-veined dolomites are green and orange/brown.

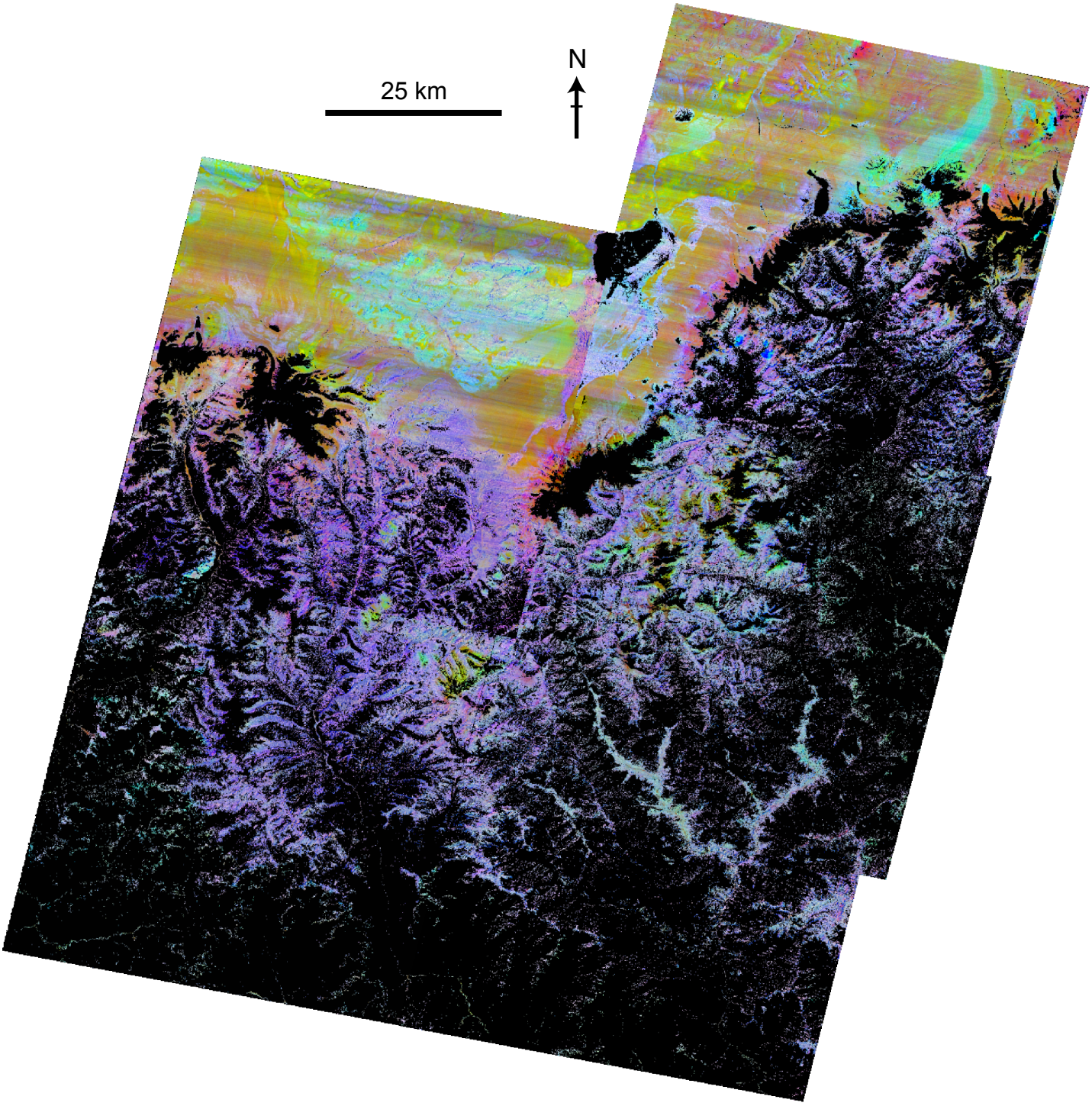

Cooper et al. (2012): Large normal-sense displacement on the South Tibetan fault system in the eastern Himalaya

GSA Data Repository Item DR5

Decorrelation stretched emissivity mosaic of the seven masked (water, ice, and vegetation removed) ASTER AST05 scenes constructed from the thermal infrared bands 10 (8.125-8.475µm), 12 (8.925-9.275µm), and 14 (10.95-11.65µm) mapped as red, green, and blue, respectively. In this stretch, the bands were chosen to highlight the spectral variability in the mountainous regions of the image where pelitic and gneissic rocks are green, and calcareous marbles and quartz-veined dolomites are pink and blue.

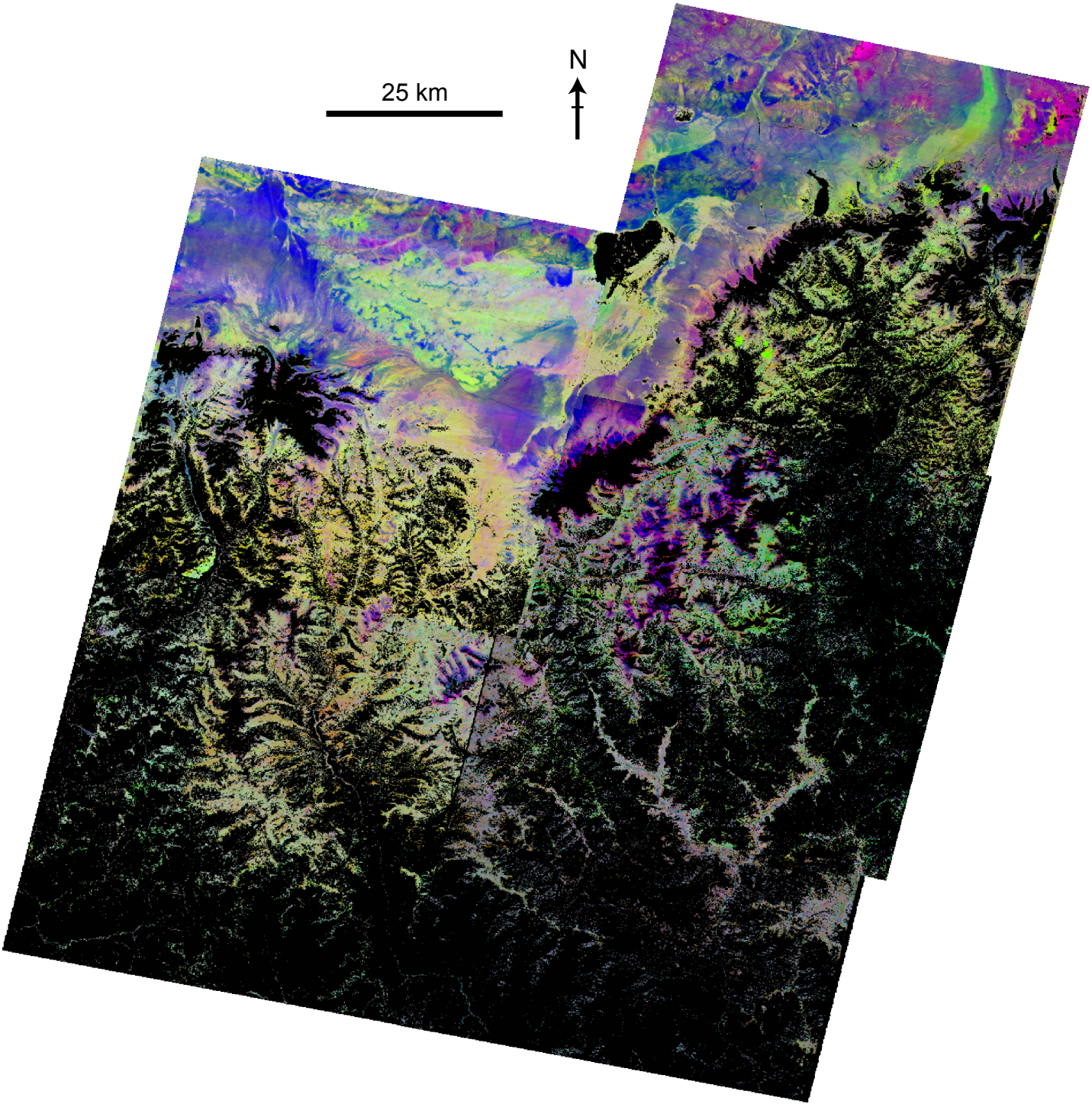

Geographically referenced versions of the geologic map as:
-an ESRI ArcGIS shapefile (.lyr)
-and a Google Earth™ file (.kmz)